Critical Reviews™ in Biomedical Engineering, 41(3):183–204 (2013)

Compressed Sensing MRI: A Review

Sairam Geethanath,[1,*] Rashmi Reddy,[1] Amaresha Shridhar Konar,[1] Shaikh Imam,[1] Rajagopalan Sundaresan,[2] Ramesh Babu D.R.,[1] & Ramesh Venkatesan[2]

[1]Medical Imaging Research Centre, DSCE, Bangalore, India; [2]Wipro-GE Healthcare, India

*Address all correspondence to: Sairam Geethanath, Ph.D., Director, Medical Imaging Research Centre, Dayananda Sagar College of Engineering, Bangalore, India; Tel.: +91-80-42161733; Sairam.Geethanath@dayanandasagar.edu

ABSTRACT: Compressed sensing (CS) is a mathematical framework that reconstructs data from highly undersampled measurements. To gain acceleration in acquisition time, CS has been applied to MRI and has been demonstrated on diverse MRI methods. This review discusses the important requirements to qualify MRI to become an optimal application of CS, namely, sparsity, pseudo-random undersampling, and nonlinear reconstruction. By utilizing concepts of transform sparsity and compression, CS allows acquisition of only the important coefficients of the signal during the acquisition. A priori knowledge of MR images specifically related to transform sparsity is required for the application of CS. In this paper, Section I introduces the fundamentals of CS and the idea of CS as applied to MRI. The requirements for application of CS to MRI is discussed in Section II, while the various acquisition techniques, reconstruction techniques, the advantages of combining CS and parallel imaging, and sampling mask design problems are discussed in Section III. Numerous applications of CS in MRI due to its ability to improve imaging speed are reviewed in section IV. Clinical evaluations of some of the CS applications recently published are discussed in Section V. Section VI provides information on available open source software that could be used for CS implementations.

I. INTRODUCTION

Magnetic resonance imaging (MRI), as a biomedical imaging modality, provides images with excellent soft tissue contrast. MRI has been extensively used to image detailed structure, function, and metabolism of the organ of interest. The reduction of MRI acquisition time is an ongoing challenge to enable imaging of certain biological processes that demand high spatial and/or spectral resolutions. To achieve short acquisition times, techniques such as PI (Ref. 1) and other undersampling strategies such as keyhole imaging have been accomplished. These techniques are typically governed by the Nyquist sampling rate and hence cannot yield acceleration beyond the Nyquist limit due to the resulting aliasing artifacts and their ability to resolve them in cases of reduced signal-to-noise ratio (SNR). A mathematical framework called CS that has been proposed,[2] provides for reconstruction of data from highly undersampled measurements.[2,3] CS has been applied to MRI to gain acceleration in acquisition time and it has been demonstrated on diverse MRI methods. Recently, it is also been used in clinical applications for pediatric imaging where reduction in acquisition time is critical for diagnosis.[4] The following subsections discuss the fundamentals of CS.

A. Sparsity

A vector is said to be "sparse" if the majority of its coefficients are equal to zero and very few coefficients will contain all the information. If significant numbers of these coefficients are exactly zeroes, then the sparsity is said to be "strong." Generally, there exists a transition band from the few high-valued coefficients to the many zero-valued coefficients, which is called "weak sparsity." From a signal processing standpoint, a sparse signal has most of its energy contained in a few measurements while the rest of the measurements are zero or negligible.

1. Transform Sparsity and Compression

Transform sparsity results in a vector, which becomes sparse on using a mathematical transform. For example, a voltage depicting a sinusoidal characteristic of a particular frequency when recorded over time does not exhibit sparsity. However, on the use of Fourier transform, the transformed vector has all of its information in two peaks ($\omega \pm \omega_o$). Now,

1040-8401/13/$35.00

the sine wave is said to be sparse in the Fourier domain. Most MR images are sparse in some transform domain. For instance, angiography images are sparse in the identity and finite differences domains whereas cardiac cine images are sparse in the spatiotemporal Fourier domain.

Sparsity can also be extended to compressibility, wherein the important coefficients that could be used for reconstruction of the original signal could be retained. Threshold is applied in the region where there is a sharp decrease in the amplitude of the coefficients when they are sorted in a descending fashion. This threshold decides the number of coefficients to be used to reconstruct. It indicates the cut-off for the important coefficients from the less important ones (analogous to the cut-off frequency for impulse response filters in signal processing). Generally, the wavelet transform is most ubiquitously used to compress the images. The reconstruction of the images is done from the sparse coefficients. If this reconstruction is exact, the image is said to be compressed with no losses, i.e., the difference between the original and reconstructed images from compressed data is zero. If this is not the case, the compression is said to be "lossy." Lossy compression results in loss of some information that is typically not perceivable to the human eye. This information corresponds to the coefficients closer to the zeroes and is not used for reconstruction. This is applicable to MR images as well. However, it should be noted that lossy compression in certain medical imaging applications involving detection problems might not be tolerable and have to be evaluated by radiologists.

2. CS: The Idea

The conventional method of image compression is performed after the acquisition of the entire image, which typically involves wavelet transforming of the image. Compression is done to accomplish saving in data storage and to facilitate the transfer of such data. Hence, the compressed data consists of only the most important coefficients that enable near-perfect reconstruction of the original data.

The philosophy of CS is to acquire only the important coefficients of the signal during the acquisition by compression and by using the concept of transform sparsity rather than compression postacquisition. The implementation of an ideal CS solution is given by the answer to a simple question: What is the minimum number of coefficients in a transform domain required to acquire data with acceptable SNR and high data fidelity to represent the object of interest?

3. The L_0, L_1, and L_2 Norms

The above question raised in Section I.A.2 can be mathematically cast as an optimization problem. The first half of the question would be to solve for the minimum number of coefficients in the transform domain required to achieve exact reconstruction. The "norm" function in linear algebra can be used to evaluate this criterion. The L_p norm of a vector x of length n is expressed as follows:

$$||x||_p = \left(\sum_{i=1}^{n} |x_i|^p \right)^{1/p} \quad (1)$$

In the case of $p = 0$, called the L_0 norm, (1) simplifies to the number of nonzero elements in the vector (n in the case of a vector consisting of ones), which is the required solution. The L_0 norm is not convex in nature, and computationally intractable, which results in difficulty in its usage in optimization problems.[5] However, L_0-based CS reconstruction has been reported recently that utilizes nonconvex optimization schemes.[6] Mathematically, solution to a convex problem or an approximately convex problem is more stable than a nonconvex optimization scheme due to reliability in convergence. Hence, the next integer ($p = 1$) norm L_1 is generally used, which is a convex approximation for L_0 norm and provides the absolute sum of the elements of the vector. It must be also noted that reconstructions using $L_{1/2}$ and other non-integer norms utilized in a nonconvex framework have also been explored.[7] The L_1 norm penalizes the presence of a large number of components, which ensures sparsity of the solution vector. In other words, L_1 norm prefers the presence of a few coefficients, which contain the total energy of the signal, while the rest of coefficients are predominantly zeros. The second part of the CS

problem is to ensure data fidelity. The L_2 norm is an ideal choice for ensuring consistency since the norm penalizes small errors relatively lesser and large errors more significantly due to the quadratic nature of the norm. Hence, the solution to the CS optimization consists of two terms: an L_1 norm of the transform coefficients to ensure sparsity, and an L_2 norm of the measured data and its iterative approximation to account for data consistency. This paper is organized as follows: Section II reviews the requirements for the application of CS to MRI; Section III discusses various CS techniques such as acquisition and reconstruction techniques such as *k-t* FOCUSS, *k-t* BLAST, Bayesian experimental design, *k-t* group sparse, modified CS (MCS), motioncompensated MCS (MC-MCS), and combination of CS and PI methods such as SparseSENSE, phase-constrained CS (PC-CS) reconstruction, L_1-SPIRiT reconstruction techniques, and the mask design problems; Section IV explores various applications of CS, i.e., cardiac MR, dynamic contrast enhanced MRI (DCE-MRI), angiography, functional MRI (fMRI), MR parameter mapping, diffusion-weighted imaging (DWI), arterial spin labeled (ASL), musculoskeletal system, and magnetic resonance spectroscopic imaging (MRSI); Section V discusses the clinical evaluation of some of the CS applications; and Section VI provides a few resources for open source software that could be used for CS implementations.

II. REQUIREMENTS FOR APPLICATION OF CS TO MRI

The implementation of CS to MRI is relatively straightforward. Here, one has to have a prior knowledge of the type of MR images he/she is going to acquire so that certain unique properties of that particular class of images can be utilized optimally, which is not a challenge since this information is typically known. For instance, the person obtaining an MR angiography image will know that the images resulting from MR angiography (MRA) will also be sparse in its native representation. This prior knowledge provides an idea to the CS implementer about the utility of application of CS to that of MR method. As already mentioned, MRA is sparser in the finite difference domain or the total variation (TV) norm. There are three fundamental requirements for the application of CS to MRI, detailed below.

A. Transform Sparsity

The fundamentals of transform sparsity have been described in section I.A.1. It is one of the three most important requirements for the implementation of CS. However, choosing the right transform to exploit sparsity existing in a particular class of MR images is a challenging task and is a field of ongoing research. Hence, to achieve the purpose, 2D or 3D wavelets are generally used, since wavelets result in good compression of medical images. Also, it is required to find an optimal solution to explore the best transform sparsity for each particular case. Dynamic contrast enhancement MRI (DCE-MRI) is one of the examples wherein spatiotemporal correlations can be exploited to increase transform sparsity along with the use of wavelets. Thus, the transform sparsity is one of the requirements that allow the CS implementer to evaluate the sparsity of the images and it also provides an insight into the number of samples he/she needs to acquire to achieve exact reconstruction, which is completely dependent on the number of sparse coefficients that are enough to result in an exact reconstruction (Fig. 1).

B. Pseudo-Random Undersampling

An MRI scanner collects the spatial frequency information, which is called *k*-space. To apply CS to MRI, the collected *k*-space has to be randomly undersampled so that aliasing artifacts are not produced due to the nonprime nature of the vector size (Theorem 1.1, in Ref. 2) as noticed in the case of sub-Nyquist sampling. A randomly undersampled *k*-space, as shown in Fig. 2, results in artifacts that are incoherent with the image and can be denoised to obtain the original image. The samples required to be acquired are typically five to eight times the number of sparse coefficients of the data set.[2] Hence, the sparser the transformed data, the fewer the samples required to reconstruct. Random undersampling of *k*-space has two specific practical limitations and/or considerations. One of the limitations is that it is

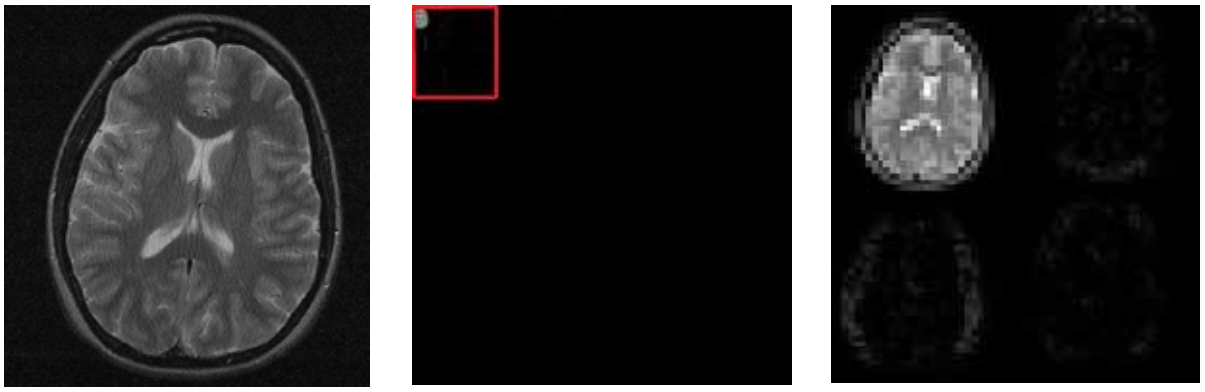

(a) (b) (c)

FIGURE 1. Transform sparsity: (a) a 2D MR image of the human brain; (b) representation of the object in 2D Daubechies wavelet transform domain; (c) a magnified view of the wavelet coefficients shown in the red square in (b)

(a) (b) (c)

FIGURE 2. Random sampling: (a) *k*-space of the brain image shown in Fig. 1(a); (b) a sampling mask showing the sampling locations of the *k*-space as white pixels while the black pixels represent unsampled locations; (c) the resulting minimum energy reconstruction demonstrates the resulting incoherent artifacts

difficult to achieve pure random *k*-space sampling since it requires rapid switching of gradients, which is impractical due to the resulting eddy currents and related artifacts.

The second consideration arises from the fact that most of the energy of the data acquired is located in the low-frequency components. Hence, a uniform weighting of the samples would result in reduced SNR. To overcome these limitations, variable density pseudo-random sampling schemes have been proposed and successfully implemented.[8] The variable density pseudorandom sampling mask consists of more samples in the center, with fewer samples in the edges. This prevents the loss of SNR but it requires optimal gradient design and new *k*-space trajectories to sample the chosen points in *k*-space. Another approach to retain the SNR is to start from conventional *k*-space trajectories and then introduce incoherent sampling in the same framework by skipping phase encode values, as demonstrated in Ref. 8.

A major factor in the implementation of CS with regard to undersampling is the dimensionality of the data. MR images with higher dimensionality (3D or higher) provide better sparsity (similar to

image compression) and hence these images yield better CS performance, i.e., CS technology is better suited to accelerate MR acquisitions of higher-dimensional data. This is ideal since MR scans involving higher-dimensional data are the ones that are the most time consuming.

C. Nonlinear Reconstruction

The constrained optimization problem put together in Sections II.A and II.B can be described by the following equation (reproduced from Ref. 3):

$$\text{minimize}||\psi m||_1$$

$$\text{s.t.}\,||F_u m - y||_2 < \varepsilon \qquad (2)$$

where m is the desired image, y is the measured k-space data, Ψ is the sparsifying transform, and ε is the parameter for error tolerance. This equation can be recast as an unconstrained optimization problem using the Lagrange method as shown in Eq. (3). Here, λ is the regularization parameter that needs to be chosen to balance the data consistency and sparsity terms. Equation (3) can be solved using an iterative nonlinear reconstruction method (see Fig. 3). Along with various available methods such as subspace pursuit, steepest descent method, etc., the nonlinear conjugate gradient has been well studied and applied.

Briefly, the nonlinear conjugate gradient (NCG) calculates the direction of the gradient, which is given by the differentiation of the above equation. At each step, the length of the step to be taken in the gradient direction is given by a line-search parameter. The stopping criteria for the iterations are twofold, as follows:

1. The difference of values of the tolerance parameter between successive iterations is negligible
2. The value of the tolerance parameter is smaller than the chosen ε value

The precise number of iterations is problem dependent, but the limiting number of iterations for an NCG solution is defined. The reconstructed image m obtained at the end of this process is the desired solution to the following.

$$\text{argmin}_m||F_u m - y||_2^2 + \lambda||\psi m||_1 \qquad (3)$$

III. COMPRESSED SENSING TECHNIQUES

A. Acquisition and Reconstruction

CS has made a significant impact in the field of MRI to minimize the image acquisition time in the last few years.[3] CS in MRI uses the Fourier coefficients (k-space samples) to make accurate reconstructions

(a) (b) (c)

FIGURE 3. Nonlinear reconstruction: (a) k-space of the brain image shown in Fig. 1(a); (b) a variable density sampling mask showing the sampling locations of the k-space with 33% sampling; (c) the resulting image reconstructed iteratively using Eq. (3) implemented via NCG

from a small subset of *k*-space rather than an entire *k*-space data. Some MR images are sparse in the pixel representation and other images could have sparse representations in the wavelet transform domain. According to CS theory, images with a sparse representation can be recovered from randomly undersampled *k*-space data. MR images need to be transformed to a sparse domain to enable CS reconstruction. We will discuss different CS techniques in the following paragraphs.

1. k-t FOCUSS

k-t space FOCal underdetermined system solver (FOCUSS)[9] starts by finding a low-resolution estimate of a sparse signal, and then this solution is pruned to a sparse signal representation. This technique uses the previous iteration solution to implement the pruning process by scaling the current solution. Once some entries of the previous solution become zero, then these entries will be fixed to zero values. This method obtains a sparser solution with more iterations. These entries corresponding to the zero values on the original spectral support converge to zero during this pruning process. Hence, one of the important requirements of FOCUSS is a reasonable lowresolution estimate that provides the necessary extra constraint to resolve the nonuniqueness of the problem.

2. k-t BLAST

The only prerequisites for *k-t* broad-use linear acquisition speed-up technique (*k-t* BLAST) reconstruction are spatiotemporal correlations to be present in the data, and these correlations to be accurately captured by the training scan. The training scan is the low-resolution scan acquired at the full temporal bandwidth, which is performed either before (for periodic motion) or interleaved with the actual data acquisition. Training data have been used to resolve aliasing from undersampling along the spatial and temporal dimensions very efficiently. In this technique, the information about the object is actually measured rather than simply assumed, as in the view-sharing approach; this method can also be successfully applied to dynamic MRI such as cardiac imaging or inflow imaging.[10]

In dynamic MRI, data sparsity was introduced by applying the Fourier transformation along the temporal dimension assuming that only parts of the field of view (FOV) change at a high temporal rate while other parts change slowly or remain stationary.[10] CS was achieved by randomly skipping phase-encoding lines in each dynamic frame. Cardiac cine data and Fourierencoded velocity data of the carotid artery were used to test the reconstruction performance.

The *k-t* BLAST results in inhomogeneous distribution of error with largest errors occurring at locations corresponding to dynamic object edges. In contrast, the error in CS is more homogeneously distributed and smaller for highly dynamic object features.

Spatiotemporal resolution is one of the quality-measuring metrics in dynamic MRI such as cardiac cine imaging or functional MRI. It was very difficult to acquire a whole volume image within a single breath hold. Various techniques were developed using parallel coil and temporal filtering to overcome these issues. Simultaneous acquisition of spatial harmonics (SMASH), generalized autocalibrating partially parallel acquisitions (GRAPPA), partially parallel imaging with localized sensitivities (PILS), and sensitivity encoding (SENSE) belong to PI techniques and unaliasing by Fourier-encoding the overlaps using the temporal dimension (UNFOLD) to remove aliasing using temporal filtering. But still these techniques have low SNR, and aliasing artifacts at high reduction factor, these drawbacks are overcome by using the model-based methods such as *k-t* BLAST/SENSE and *k-t* FOCUSS.

3. k-t FOCUSS for Dynamic MRI

The *k-t* FOCUSS technique has also been applied to dynamic MRI, and it has been shown to perform better than the *k-t* BLAST with the following advantages:

1. *k-t* FOCUSS minimizes the L_1 norm, which is optimal from the CS perspective, but *k-t* BLAST does not minimize the L_1.
2. Image estimation depends on the parameter p and value of which is 1 in *k-t* BLAST but this restriction is re-

laxed in *k-t* FOCUSS, and any value between 0 to1 can be used. $p = 0.5$ in *k-t* FOCUSS performs better in stability and reconstruction quality than the $p = 1$ in *k-t* BLAST.

In this technique, temporal average contributions are first subtracted from *k-t* samples and which are converted to the *x-f* domain using the Fourier transform. The weighting function calculated from the equation 15 in Ref. 11 was used first time. A power factor between $0.5 < p < 1$ has been used for the reconstruction. Solution for $p = 1$ was too sparse. $p < 0.5$ was not able to remove aliasing artifacts and choice of value $p = 0.5$ seems optimal in many applications once the weighting matrix is constructed. The *k-t* FOCUSS algorithm was used for high-resolution dynamic MRI because it showed that *k-t* FOCUSS was optimal from a CS perspective.[12] A method was proposed based on the extension of *k-t* FOCUSS to a more general framework, in which the prediction provides initial encoding and residual encoding takes care of the remaining residual signals. This technique uses a motion estimation and compensation scheme for sparsifying the signals and also provides the best undersampling pattern for CS. The proposed method uses the idea from video compression and the MPEG standard.

Non-Cartesian k-space trajectories were used for the undersampling of *k*-space to accelerate acquisition. Optimization of the *k*-space trajectory for sparse nonlinear reconstruction was one of the challenges in CS and the mask designing problem is discussed in further detail in Section III.C. This has resulted in the Bayesian approach for mask design.

4. Bayesian Experimental Design

The objective discussed in the previous section has led to the Bayesian experimental design. Bayesian experimental design was used for optimization of k-space trajectories for CS.[13] The technique was proposed for the reconstruction of sparse MRI signal using standard signal processing primitives for the efficient use of *k*-space trajectories, which was demonstrated for Cartesian and spiral but also extendable. Further, the mask design problems are discussed in Section III.C in detail.

Multiple acquisitions of the same region of interest under several different contrast preparations are done in clinical imaging with structural MRI.[14] Reconstruction algorithm based on Bayesian CS to jointly reconstruct a set of images from undersampled *k*-space data with higher fidelity than when the images are reconstructed either individually or jointly. Image gradient coefficients are calculated for each image. All of the images from the same anatomical region, but with different contrast properties, contribute to the estimation of the hyperparameters, and variance of image gradients across contrasts for a single volumetric spatial position is single hyper-parameter. The *k*-space data belonging to each image are used independently to infer the image gradients. Thus, commonality of image spatial structure across contrasts is exploited without the problematic assumption of correlation across contrasts.

CS reconstruction for dynamic cardiac MRI has been improved by incorporating additional information on the support of the dynamic image in *x-f* space based on the theory of CS with partially known support by using technique *k-t* iterative support detection (*k-t* ISD).[15] This technique uses an iterative procedure for alternating between image reconstruction and support detection in *x-f* space. Support information from the previous iteration was used to apply a truncated L_1 minimization to obtain the reconstructed image in *x-f* space. The method alternates between CS reconstruction with partially known support (PKS) and adaptive learning of support knowledge used in the next iteration by thresholding the reconstruction.

Another CS technique proposed to accelerate the dynamic MRI, which makes use of the structure within the sparse representation of a signal by enforcing the support component in the form of groups, is called *k-t* group sparse.[16] Support estimation, group assignment, and signal recovery are the three key steps in this technique. In this work, a training scan was used to identify the support region in the *x-f* space. A threshold is set above the noise level in the *x-f* space and elements with intensities above the threshold constitute the support region, then support in *x-f* space is estimated from the previous step to assign elements in *x-f* space to distinct groups. Once the groups are assigned to all elements

in the *x-f* space, the signal recovery is done by the group sparse formulation. However, the use of this technique in dynamic MR applications has been limited in terms of the maximum achievable reduction factor. In general, noiselike artifacts and bad temporal fidelity are visible in standard CS MRI reconstructions when high reduction factors are used. To increase the maximum achievable reduction factor, additional or prior information can be incorporated in the CS reconstruction. This technique exploits the structure within the sparse representation of a signal by enforcing the support components to be in the form of groups. These groups act like a constraint in the reconstruction. Figure 4 depicts an illustration of the group assignment step of the proposed method (a: 8 × 8 sparse image, b: group assignment matrix showing the group number to which element/pixel at the respective location is assigned).

The iterative soft thresholding (IST) framework has been used for accelerated MRI using CS.[17] This technique is data driven and no tuning of free parameters is required. A Nesterov-type optimal gradient scheme for iterative update along with standard wavelet-based adaptive denoising methods were combined, which results in a leaner implementation compared with the nonlinear conjugate gradient method. The technique was evaluated on T_2 weighted brain data, and vascular 3D phase contrast data show that the image quality of reconstructions is comparable with those from an empirically tuned nonlinear conjugate gradient (NLCG) approach.

5. Modified CS

In modified CS, it is assumed that the support (location of nonzero coefficients) of the signal in the sparse domain is partially known and can be used in reconstructing the sparse coefficients with greater accuracy.[18] Partial knowledge of the signal support can be found a priori in many signal processing applications. For example, it is common knowledge that the locations of the significant Fourier coefficients of the signal are present at the lower frequencies. Such partial knowledge, when introduced into an L_1 minimization objective, results in a sparser solution that is better than conventional CS solutions at high acceleration factors. Thus, the modified CS problem introduces the partial support information and aims to find the sparsest signal outside the known support while satisfying the data constraint.

A time series extension of this framework is named dynamic modified CS, which assumes that support changes occur slowly in the time series. Thus, the known support for reconstructing the current frame is assumed to come from the support estimate of the previous frame. This knowledge is then used in a modified CS framework to find the signal that satisfies the data constraint and is sparsest outside this known support. The dynamic modified CS algorithm is stated in Ref. 18. The dynamic modified CS works better than conventional CS at high acceleration factors. One such technique called motion-compensated modified CS combines motion estimation/compensation and modified CS to create

229	209	91	98	146	43	59	28
246	63	213	146	121	155	234	247
141	238	150	20	4	68	40	2
36	90	141	14	87	168	212	199
39	51	235	136	42	177	138	210
66	65	74	200	204	192	256	223
216	158	194	240	80	116	21	22
66	122	193	34	136	22	114	103

1	1	3	3	2	4	4	4
1	4	1	2	3	2	1	1
2	1	2	4	4	3	4	5
4	3	2	4	3	2	1	1
4	4	1	2	4	2	2	1
3	4	3	1	1	2	1	1
1	2	1	1	3	3	4	4
3	3	1	4	2	4	3	3

FIGURE 4. Formation of groups using threshold values

an algorithm that aims to improve the modified CS reconstruction.

6. Motion-Compensated Modified CS (MC-MCS)

The dynamic modified CS algorithm heavily relies on the assumption that signal support changes slowly over time, i.e., dynamic MCS works well. This assumption is violated in image sequences as presence of motion causes significant changes in the support set of adjacent image frames. If these motion differences can be corrected, the modified CS framework can be exploited to provide more accurate support information. In Ref. 19, motion estimation and compensation methods frequently used in video processing were used to correct for motion and provide a better estimate of the support.

For MC-MCS, two inputs are required, i.e., a noisy measurement and the desired number of motion compensation iterations. The reconstructed signal $\widehat{Xt}$ is the output. The dynamic MCS is run to calculate estimates of the sparse representation $\widehat{Xt}$ for all *t*. Initially, the estimate of the image frame is calculated and corresponding vectors are computed. Then, the calculated values are updated.

B. Combination of CS and PI

As already mentioned, CS can improve the spatial and/or temporal resolution of the acquired images by reducing the number of necessary samples for image reconstruction. Using CS, a sparse signal can be recovered from very few samples and thus reduces the scan time without the requirement of improved gradient performance.[20]

Parallel MRI (pMRI) is a method that is used to reduce the acquisition time by using multichannel receiver arrays to acquire the MR signal simultaneously from several receiver coils, which provides a substantial increase in imaging speed.[21] Data received simultaneously by several receiver coils with distinct spatial sensitivities are used to reconstruct the values in the missing *k*-space lines. In pMRI, the number of samples is reduced using multiple channels for simultaneous data acquisition. The reduction in the number of samples is limited by the number of channels and SNR. The application of CS to PI has been investigated to achieve an even higher imaging speed.

3D MRI is one of the important areas for investigation of anatomy, function, and pathophysiology. 3D imaging provides the quantitative volumetric information of the region of interest when scanned. 3D MRI scans can be accelerated by using time-efficient sampling, undersampling of *k*-space, and advanced reconstruction methods that remove aliasing artifacts.[22] PI can effectively remove aliasing artifacts by the use of appropriate receiver coil arrays. By combining PI with CS, this purpose can be achieved. Here, a phase-constrained CS (PC-CS) reconstruction to imaging with multichannel receiver coil arrays (PI) was applied, which first estimates phase maps for each coil element, and then reconstructs the final image iteratively. Multicoil PC-CS reconstruction was performed by knowing the estimates of the phase and magnitude coil sensitivity maps.

L_1-SPIRiT reconstruction is one of the methods to reconstruct MR images using the CSPI framework[23] involving the combination of CS with PI. It is a compressive sensing extension to the SPIRiT (iterative self-consistent parallel imaging reconstruction) PI reconstruction. SPIRiT is based on GRAPPA but takes slightly different approach compared to GRAPPA. The approach splits the consistency term into two: consistency with data acquisition and consistency with calibration.

1. L_1 Regularization

Consider the optimization problem,

$$\text{argmin}_m ||Dx - y||^2 + \lambda_1(||(G-I)x||^2 + \lambda_2 R(x) \quad (4)$$

Function $R(x)$ is a penalty function that gives prior knowledge. The above formula is very flexible because the penalty can be applied on the image as well as *k*-space data. Taking W as a data weighting function, $\nabla\{\}$ as a finite-difference operator, and $\Psi\ \{\}$ as a wavelet operator, here are some examples of potential penalties:

$R(x) = ||x||_2$, Tikhonov regularization

$R(x) = \|Wx\|_2$, weighted Tikhonov regularization

$R(x) = \|\nabla \{\text{IFFT}(x)\}\|_1$, total variation (TV)

$R(x) = \| \Psi \{\text{IFFT}(x)\}\|_1$, $\ell 1$ wavelet.

The last two are L_1 penalties and are very much popular due to the theory of CS. The data were processed in the following way. Each data set was reconstructed several times using traditional GRAPPA, each time with a different kernel size (5×5, 7×7, and 9×9).[24] The GRAPPA kernels were calibrated for each unique local sampling pattern set. In addition, each data set was reconstructed using the k-space-based Cartesian SPIRiT with equality data consistency, again with 5×5, 7×7, and 9×9 kernel sizes. The SPIRiT reconstruction was implemented using the LSQR conjugate gradient algorithm. To show the dependency of the reconstruction on the number of iterations, the results at the sixth, eighth, tenth, twelfth, and fourteenth were saved.[24] Finally, each data set was reconstructed with SPIRiT with L_1-norm wavelet regularization. The wavelet regularization parameter was empirically set to 0.015. For each of the above experiments, the resulting reconstructed coil images were combined with the square root of the sum of squares. Once the reconstructions were completed, the mean difference error with the fully sampled data set was calculated. The standard deviation for each pixel across the 100 scans was computed and normalized by the standard deviation of the pixels in the full set (taking into account the reduced scan time) to obtain empirical noise amplification (g-factor maps) estimates.

L_1-SPIRiT provides accelerated sampling, reconstruction, and the incoherence required for CS, which is also compatible to PI. SENSECS and CSSENSE are the methods that perform the overall reconstruction in two cascading steps. SENSECS is an application of CS in parallel MRI. It exploits both the image sparsity and coil sensibility encoding[25] by exploiting the complementary characteristics of SENSE reconstruction and CS reconstruction. In SENSECS, SENSE is used to obtain an image estimate and then the artifacts are removed by using the prior estimate. In CSSENSE, CS is first used to obtain intermediate stage aliased images whose aliasing artifacts are removed by SENSE. SENSECS outperforms CSSENSE due to the fact that the final CS stage reconstruction in SENSECS is more error forgiving than the final stage SENSE reconstruction in CSSENSE. Also, SENSECS is more computationally efficient in terms of sampling pattern design and image reconstruction.

C. Mask Design Problems

CS can reduce imaging time in many MRI applications significantly by lowering the number of samples taken for image reconstruction. Samples are selected based on the sampling trajectories. The time course of filling up the lines in *k*-space is called the *k*-space trajectory. There are diverse types of sampling trajectories such as Cartesian, radial, and spiral trajectories, as shown in Fig. 5.

The most commonly used trajectory is the Cartesian grid since it is robust in data collection while also being very practical to implement and simple to reconstruct.[8,26] However, there are certain medical imaging applications that require high spatial and/or temporal resolutions. Cartesian imaging does not provide the adequate solution to such necessities since it gathers the data with a uniform weighting throughout the Cartesian grid. In application for CS, Cartesian trajectories show to be coherent, compared to random *k*-space sampling. The non-Cartesian approaches (radial and spiral) can be used to gain higher SNR since the sampling of the center of k-space typically determines the SNR. The density of *k*-space is however nonuniform since most of the information is typically contained in the low-frequency components that are in the center of the k-space rather than the high-frequency components that lie toward the edges of the grid. This has given rise to research on non-Cartesian trajectories. The radial acquisitions are less susceptible to motion artifacts than Cartesian trajectories and can be significantly undersampled.[8] In the case of spiral trajectory, gradient system hardware is efficiently used. This trajectory is used for real-time and rapid imaging applications. The approach of utilizing trajectories suited to the density of the *k*-space aids in quicker sampling of the more important data points and hence reduces acquisition time. The sampling mask

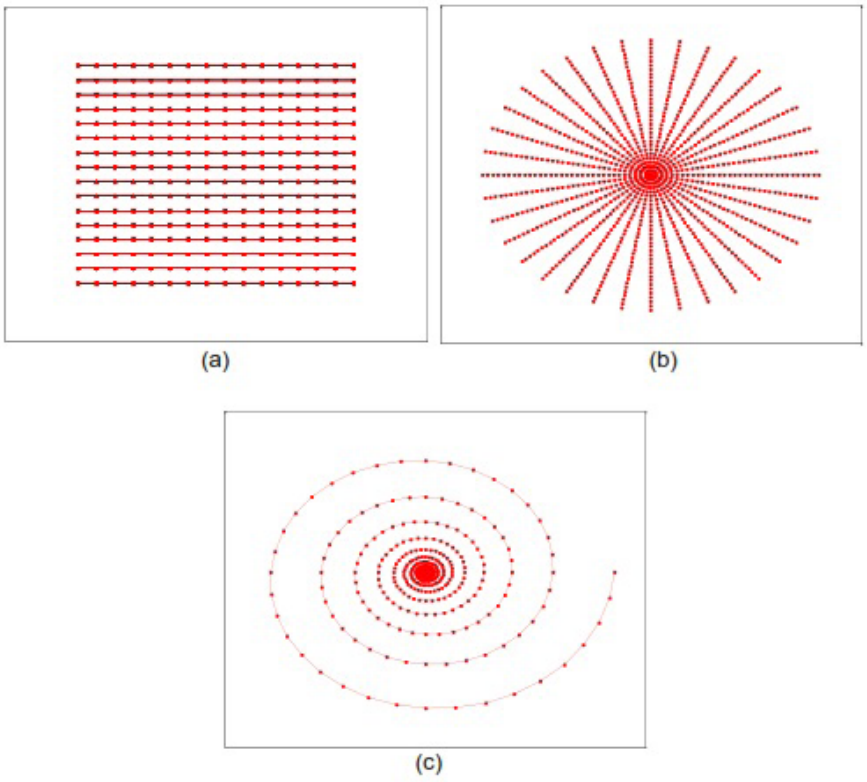

FIGURE 5. *k*-space trajectories: (a) Cartesian; (b) radial; (c) spiral with increased sampling in the center

is created by a matrix of ones and zeroes. The mask will sample the *k*-space only where its value is 1. Consider the mask shown in Fig. 6. It is a random mask with pink dots representing ones and blue dots representing zeroes. The mask samples the *k*-space only where its value is $1\delta(u - u_j, v - v_j)$.

Figure 6 shows the original PSF and the corresponding reconstructed PSFs obtained by applying a random mask, uniform mask, Poisson mask, and variable density mask, respectively. From Fig. 6, we can observe that as the randomness in the mask increases, the aliasing artifacts reduce.

IV. APPLICATIONS OF COMPRESSED SENSING

A. Cardiac MR

Diseases of the heart including myocardial infarction (MI) and heart failure continue to be a leading cause of morbidity and mortality.[27] Cardiac MRI (CMR) gives high resolution as well as high soft tissue contrast. CMR is used to image the heart in terms of LV structure and also to identify the extent of MI (Ref. 28) and to measure myocardial perfusion. In myocardial perfusion imaging by magnetic resonance, MR contrast agent injected into the myocardium is monitored over time and has become as an alternative to the traditional technique such as single-photon emission computed tomography (SPECT). The major constraints of cardiac perfusion imaging are temporal and spatial resolution. These constraints on MR imaging speed may be reduced by use of the PI technique. Another approach for accelerated imaging is compressed imaging.[29]

The work reported in Ref. 29, i.e., fourfold accelerated cardiac perfusion MRI, has been demonstrated with the CS technique exploiting the sparsity of the dynamic image set in *x-f* space and applying *k-t* random undersampling. A joint reconstruction approach named *k-t* JOCS (joint CS) using Fourier transform in time and spatial total variation was pro-

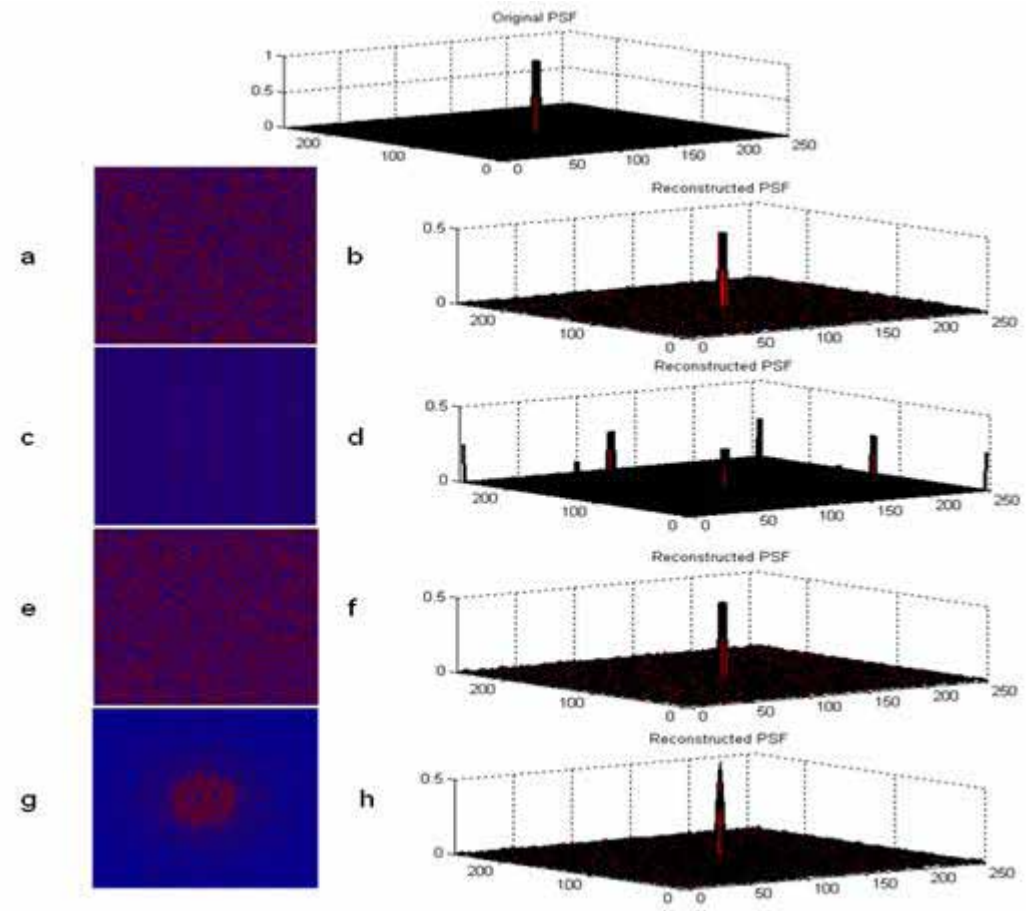

FIGURE 6. (a) Random mask; (b) reconstructed PSF using (a); (c) uniform mask, (d) reconstructed PSF using (c); (e) Poisson mask; (f) reconstructed PSF using (e); (g) variable density mask; (h) reconstructed PSF using (g)

posed[30] to combine CS and PI for highly accelerated cardiac perfusion MRI.

Therefore, a regularization parameter can be chosen to minimize the RMSE of spatial signal in ROI. The overall image quality is reduced with larger noise level 0.000121. Thus, CS can be used in cardiac MR and also TV in CS provides better regularization when the overall image quality is concerned compared to wavelet-based regularization. It must also be noted that always using the RMSE of overall signal is not the best method, since the reconstruction fidelity of ROI is required (see Table 1).

B. Dynamic Contrast Enhanced MRI

Dynamic contrast enhanced (DCE) magnetic resonance imaging (MRI) is an effective noninvasive tumor diagnosis method. In this method, images are obtained before and after the contrast agent is injected, and the number of images is obtained typically at uniform time intervals. The quantitative analysis of this agent obtained from different images gives useful information about pharmacokinetics, which can be used to characterize tumors (malignant and benign).[31]

In order to obtain DCE-MRI images, high temporal and spatial resolutions are required. Spatial resolution provides morphological information of tumors, and temporal resolution is required for kinetic analysis. A fast imaging technique is therefore required to acquire DCE-MRI images. CS has been effectively used for dynamic MRI.[32] In this CS method, a reference image is required before the contrast agent is injected. The dynamic data frames

TABLE 1. RMSE for the overall signal (RMSE-All) and for the averaged ROI signal (RMSE-ROI) when each method is optimized to minimize the overall RMSE and ROI RMSE (from Ref. 30)

Method	Optimized for overall		Optimized for ROI	
	RMSE-All	RMSE-ROI	RMSE-All	RMSE-ROI
TV	0.0228	0.000121	0.0284	0.000109
DWT	0.0408	0.000150	0.0665	0.000055
DFT	0.0289	0.000133	0.0348	0.000121

are undersampled randomly and can be used to acquire more images per unit time.[32] The image can be reconstructed from the dynamic image using the following model:[32]

$$\varepsilon(I_{\text{diff}}) = ||FI_{\text{diff}}||2 + \lambda L_1|WI_{\text{diff}}|_1 + \lambda_{\text{TV}}(I_{\text{diff}}) \quad (5)$$

where F is the forward Fourier transform matrix, λL_1 and λ_{TV} are two regularization parameters, and W is a sparsifying transform.

Three different keyhole methods based on the shape of the sampling mask were implemented in Ref. 33. The first method contains a sequence centered at the center of the *k*-space, the second method contains the number of phase encode lines in the center of the *k*-space (key lines), and the third mask is based on the locations above a specific threshold of the absolute value of the *k*-space of the precontrast image (key thesis).

CS has also been performed on three different masks (see Fig. 7). The first mask was formed by the use of points in the *k*-space with a high density weighting at the center of the *k*-space based on a Gaussian probability distribution function (pdf). In the second method, the mask was obtained by the phase encode lines based on a Gaussian pdf, and the third mask is the same as key thresh (cs_gthresh). These masks were generated for acceleration factors of 2, 3, 4, and 5. The mean RMSE values follow the trend, key lines > key thresh > key hole > cs_gauss > cs_gthresh > cs_glines.[33] Hence, in Ref. 33, clearly it has been shown that CS can be used as a fast imaging technique in DCE MRI to obtain increased spatial and temporal resolution.

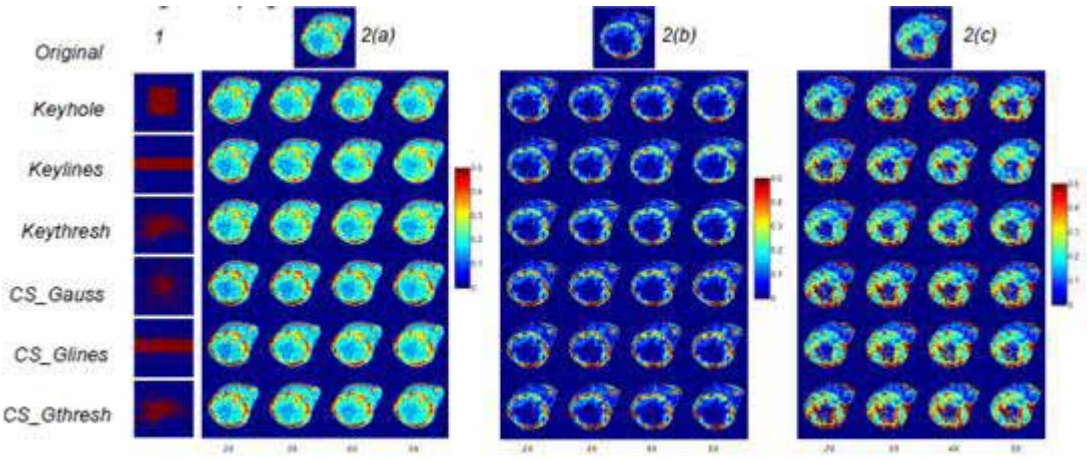

FIGURE 7. (1) Panel showing the different masks used in the study at 4*x*; (2) (a): A a post-contrast image of a representative data set of the original and for the 6 six masks at 4 four given acceleration factors, ; (b) K^{trans} Maps of the post contrast image for the original and the various masks at the given acceleration factors. ; (c) corresponding v_e maps

C. Angiography

Angiography or arteriography is a medical imaging technique used to visualize the inside, or lumen, or blood vessels and organs of the body, with particular interest in the arteries, veins, and the heart chambers. This is typically performed by injecting a contrast agent into the blood vessels and following the presence of contrast. Another MRA method is the time of flight [(TOF]) angiography, which depends on the rate of signal based on the flow-related enhancement of spins. These spins give more signal than that of stationary spins.

In angiography, important information is present in the dynamics of the contrast agent. Capturing the dynamics requires high spatial and temporal resolution. A CS-based MR angiography scan can be used to improve spatial resolution and temporal resolution by undersampling at the expense of undersampling artifacts. Angiography data is sparse in the identity transforms domain, and angiograms are sparsified very well by both wavelet transform and by finite differences.[3]

In Ref. 34, 10 reconstructions with 10 different computed undersampling masks were generated. All the masks originate from same pdf and were designed to generate a sampling pattern covering 25% of the *k*-space. NMSE was found to be 0.3 ± 0.07 for CS reconstruction and 1.37 ± 0.08 for zero filling (ZF) reconstruction. Thus, CS performs better than ZF reconstruction for low sampling rate. The quality of reconstruction was evaluated by means of NMSE for different TV weights between 0 and 10 and a sampling percentage of 25%. The value 0 gives an NMSE of 1.232, thus showing the importance of term limiting total variation. Integers ranging from 1 to 10 with increment of 1 yield an average NMSE of 0.3 ± 0.03.The NMSE decreases as sampling rate increases for both CS and ZF reconstruction. But error with CS reconstruction is much lower than the error with ZF reconstruction. Also, NMSE for image data reconstructed with CS is much lower than NMSE for MIP data reconstructed with ZF. Undersampling is required for high temporal and spatial resolution; therefore, CS reduces the artifacts due to undersampling. CS reconstruction was found to be stable with regard to the sampling pattern and reconstruction constraints, and the accuracy of CS reconstruction in angiographic data was better than the ZF reconstruction.

D. Functional MRI

Functional MRI (fMRI) is a technique to detect the activated area in the brain with respect to a given task by measuring the change of blood oxygen level dependent (BOLD) contrast. The change of BOLD signal is very small compared to the MR signal and therefore fast scans are required to prevent a noisy signal due to subject motion.[35]

fMRI has been positioned as a standard tool for the functional study of brain. fMRI using echo planar imaging (EPI) has a spatial resolution of $3 \times 3 \times 4$ mm and temporal resolution of 1–3 s. This demand of high temporal and spatial resolution requires fast acquisition time. However, typically a PI technique such as SENSE is used for accelerated fMRI. The reconstructed image using SENSE from accelerated measurements when compared with fully sampled images using conventional method gives significant difference. Therefore, a CS-based algorithm called *k-t* FOCUSS is applied to fMRI, and then the receiver operating characteristics (ROCs) of fMRI of the *k-t* FOCUSS and those of fully sampled results[36] can be compared.

As an example of fMRI, a right finger tapping experiment was performed in Ref. 36, in order to evaluate the performance of *k-t* FOCUSS in fMRI. In this method, echo planar imaging (EPI) was used with TR/TE = 3000/35 ms and flip angle = 80 deg. The *k*-space data are acquired on a 64×64 matrix size and 35 slices with 4 mm slice thickness. The number of phase encoding was reduced by two- and fourfold for each time frame while keeping the number of blocks with 10, in order to implement a high temporal resolution fMRI. A random sampling pattern was employed, the low-frequency region was fully sampled, and data were used to obtain a Karhunen-Loeve transform (KLT).

E. MR Parameter Mapping

Different tissues in the body can be distinguished in MRI by their intrinsic MR parameters such as

proton density, longitudinal relaxation time (T_1), and transversal relaxation time (T_2). The values of these parameters give more accurate diagnostic information.

But MR parameter mapping requires a long scan time due to which T_1 and T_2 are estimated only at two or three data points, thus reducing the accuracy. A higher number of measurements is required to measure the data accurately; therefore CS can be used for reducing the scan time[37] in multipoint MR parameter mapping.

In Ref. 37, T_1 and T_2 data in the brain were acquired in healthy volunteers, and measurements were performed on 1.5 *T*. Data sets were undersampled retrospectively with reduction factors of 2, 4, 6, and 8 for T_1 and 2, 3, 4, and 5 for the T_2 data set. The undersampled data were reconstructed using three different models (Nyquist sampling, conventional CS, and dictionary model[37]). The dictionary consisting of 100 atoms was trained for each model. The reconstructed images and resulting maps were compared with full sampling.

Another MR method exploiting diffusion information is diffusion weighted imaging (DWI). A specific application for DWI is neoadjuvant chemotherapy (NAC) that is administered to patients with locally advanced breast cancer to treat at an early stage. Also, NAC is offered to the patients with early stage tumors to increase the possibilities for breast-conserving surgery. During the NAC treatment, response may be monitored *in vivo*[38] to obtain individualized treatment, i.e., by modifying ineffective treatment. The early treatment response can be assessed by the use of MRI examinations. Diffusion weighted MRI (DWMRI) can be investigated as a possible predictive marker for treatment response. In DWMRI, signal attenuation depends on diffusion of water molecules in tissues. The apparent diffusion coefficients (ADCs) are calculated from two or more images with different degrees of diffusion weighting. The CS challenges for this method follow that of DTI in calculation of the parametric ADC maps.

Thus, a learned overcomplete dictionary was applied to sparsify the data, and also applied to MR relaxation parameter mapping. Hence CS reduces the acquisition time so that data can be measured in multiple points. The sparsity required for CS is obtained using a learned overcomplete dictionary.

F. Arterial Spin Labeled MRI

Dynamic MRI provides a set of morphological images and requires high special and temporal resolution. But because of the long acquisition time of MRI, either of the two has to be compromised. Therefore, many techniques have been developed to accelerate MRI; CS is found to be the best to accelerate the acquisition speed through undersampling data in the *k-t* space.

CS requires the data to be sparse in one or the other domain. There are diverse transform domains in which images appear to be sparse. All the transforms that exist are linear, but much sparser images can be obtained using nonlinear transforms leading to complicated reconstruction. The kernel-based method allows a nonlinear algorithm to be implemented in a linear algorithm.[39] This kernel-based method can be applied to dynamic reconstruction.

The performance of the kernel-based method on arterial spin labeled (ASL) perfusion data on calf muscles and myocardium in Ref. 39 was evaluated. In this method, entire *k*-space data is required and then it is randomly undersampled retrospectively. A net reduction factor of $R = 2$ was used for calf muscle data and 2.5 for myocardial data. Since the ASL-based perfusion images have abrupt variation time, it is difficult to maintain such variation in CS reconstruction. The kernel-based method as well as a conventional CS was used to reconstruct the image sequence.

G. Musculoskeletal system

A musculoskeletal system (also known as locomotor system) is an organ system that gives animals (and humans) the ability to move using the muscular and skeletal systems. The musculoskeletal system provides firm support, stability, and movement of the body. This system describes how bones are connected to other bones and muscle fibers via connective tissue such as tendons and ligaments. The bones provide the stability to a body. Muscles keep bones in place and also play a role in movement of the

bones. A long acquisition time is required to acquire muscle images in MR imaging techniques. Hence, CS is used to reduce the acquisition time.

Concurrent dephasing and excitation (CODE) is a 3D highly asymmetric radial echo MR imaging technique that allows for fast, short, T2-sensitive MR imaging with reduced motion artifacts and reduced signal dynamic range.39 CS can be used to accelerate CODE acquisitions of the human knee. The CODE MRI data is sparse in the total variation transform domain and the artifacts may be incoherent in that domain. It is important to use a 3D total variation (TV) transform to exploit the sparsity in all three dimensions and therefore it is used in the reconstruction. The following equation can be used to estimate the image:

$$\text{argmin}_m \, ||F_u m - y||22 + \lambda\text{TV} \, \text{TV}_{3D}(m) \quad (6)$$

where m is the MRI volume, y is the measured data, F_u is the undersampled Fourier operator, and λ_{TV} is the regularization parameter.

In Ref. 40, the CS CODE MRI was performed through the reconstruction on five human knee MRI data. All the data was acquired on a Siemens 3.0T Magnetom Trio. For the *in vivo* data, the TR was 3.4 ms and nominal flip angle of 5, number of projections was 128,000 (100,000 in one case), and the FOV was chosen to cover the knee, and acquired using a transceiver knee coil. Four data sets had matrix sizes of 256 × 256 × 256, while one of them had dimensions of 379 × 379 × 379. For CS reconstruction, the acquired data was undersampled through retaining projections randomly and the k-space was gridded and Fourier transformed with density compensation (*zfwdc*) and normalized. This was used as the initial estimate of the volume that was iteratively reconstructed using a custom implementation of a nonlinear conjugate gradient algorithm to solve (6) using a value of 0.005 for λ_{TV}. This value was fixed for all reconstructions of the knee data sets. This was done to ensure consistency in comparative analyses. The rms error (RMSE) weighted by the number of voxels in each data set was used to measure the error, for each acceleration factor of pooled *in vivo* data. The CS reconstruction was performed for acceleration factors of 2, 3, 4, and 5x. For solving (6), a total of 16 iterations were used. All implementations were done using Matlab, (Mathworks, Inc., Natick, Massachusetts).

The CS CODE MRI results for a human knee are shown in Fig. 8. The effect of iterative reconstruction for the CS CODE data is shown in the image. The original reconstruction (1*x*) using the full *k*-space data can be seen at the top of Fig. 8. The *zfwdc* images for acceleration factors of 2, 3, 4, and 5 are shown in the first column of images, while the second column shows the corresponding CS reconstructions. It can be clearly seen that the *zfwdc* images (a) contain incoherent noise removed by the reconstruction resulting in (b). The effect of CS reconstruction can be shown by the line intensity profile from the images shown by red line on the image and the same is shown in the adjacent graph. The magnified images of the central slice in the sagittal plane as shown in Fig. 8(c) to evaluate reconstruction of fine structures important in musculoskeletal studies. The RMSE values for the accelerations chosen for reconstruction and is <0.02 for 5x as well, as shown in Fig. 9. Thus, the application of CS to accelerate CODE MRI of the knee can be shown on five *in vivo* data sets with fivefold acceleration and reduction in noise while maintaining low reconstruction error as shown by computed RMSE values.

H. MRSI

Malignant prostrate and brain tumor are characterized by increased levels of choline. Brain tumors also lead to decreased levels of N-acetylaspartate (NAA) and creatine, which means the choline-to-NAA index can be used as a cancer biomarker. Also a biomarker for prostrate cancer is the ratio of sum of choline and creatine to citrate. The metabolic abnormality and the changes in the region originally outside the morphology lesion can be observed by using multivoxel MR spectroscopy. But a longer acquisition time is the major disadvantage of multivoxel MR spectroscopy. Hence, compressive sensing can be used in MR spectroscopy to reduce the acquisition time.

In Ref. 41, CS reconstruction was applied to 1H MRSI for *in vitro* phantom, *in vivo* brain with normal ($N = 6$), cancer ($N = 3$), and prostate cancer ($N = 2$) data sets for acceleration factors of 2, 3, 4, 5,

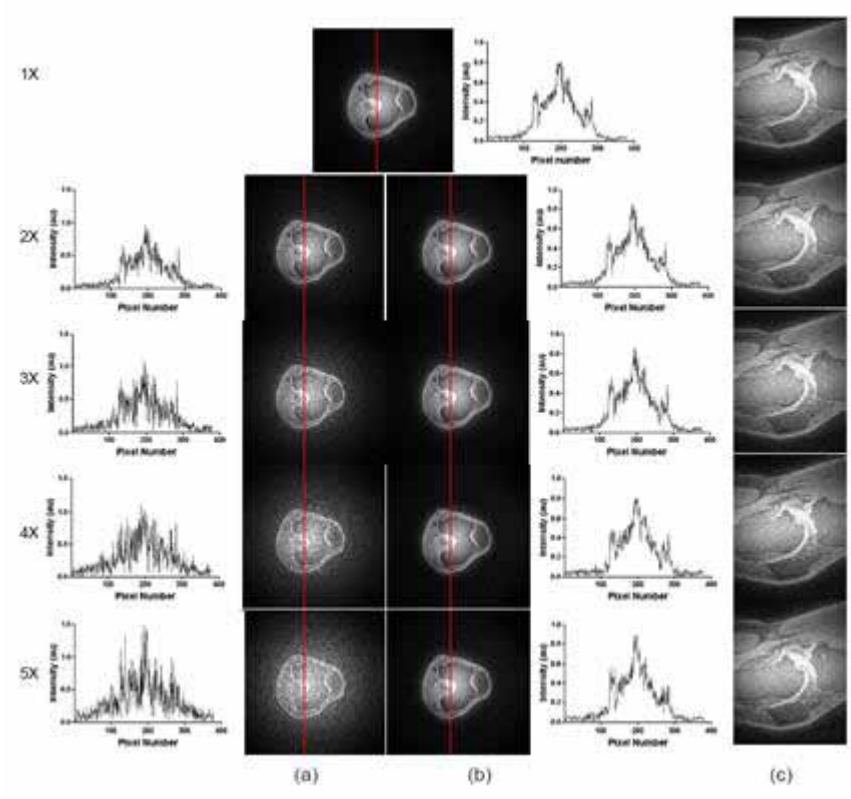

FIGURE 8. Line intensity profile of a symmetrical feature in an axial slice shown in the top panel: (a) the *zfwdc* images for the accelerations shown; (b) the corresponding reconstructions and the plot of line intensities adjacent to the images; (c) a magnified view of the original and reconstructed images of the center slice in the sagittal plane[40]

and 10. The error of reconstruction is quantified by the RMSE metric.

To evaluate the efficiency of the reconstruction, importance was given to the minimal postprocessing of the original data and reconstructed data. Following are the processing steps that were applied to the MRSI data: (a) apodization, (b) baseline correction, (c) removal of water peak, (d) zero-order phase correction, and (e) generation of metabolite maps.

Figure 10(a) shows the full *k*-space reconstruction of a prostate cancer MRSI data set. From Fig 10(b), it can be seen that reconstructed spectrum from the MRSI data set are comparable to the original data at 5*x*. The similarity between the reconstructed and the metabolite maps for the choline and citrate for both acceleration factors is shown in Fig. 10(c). Also, it can be seen that the reconstruction spectrum displays less noise compared to the original spectrum. This is because of the denoising ability of the wavelets and because of the smoothing effect of the TV in the reconstruction. Figure 11 gives the comparison of the reconstruction for different MRSI data. Clearly, it can be seen that RMSE values are <0.03 at 5*x*. The 10*x* case gives the limit of the implemented CS reconstruction technique. Thus, CS is successfully applied to different types of MRSI data and the quality of reconstruction is quantified by reconstruction error and metabolite maps that show the high fidelity compared to the original data. Therefore, these results[41] indicate that compress sensing can be used in MRSI to reduce acquisition time by 80%.

V. CLINICAL EVALUATION OF CS APPLICATIONS

Clinical evaluation of L_1 SPIR-iT (Ref. 4) was done on patients referred for routine contrast agent

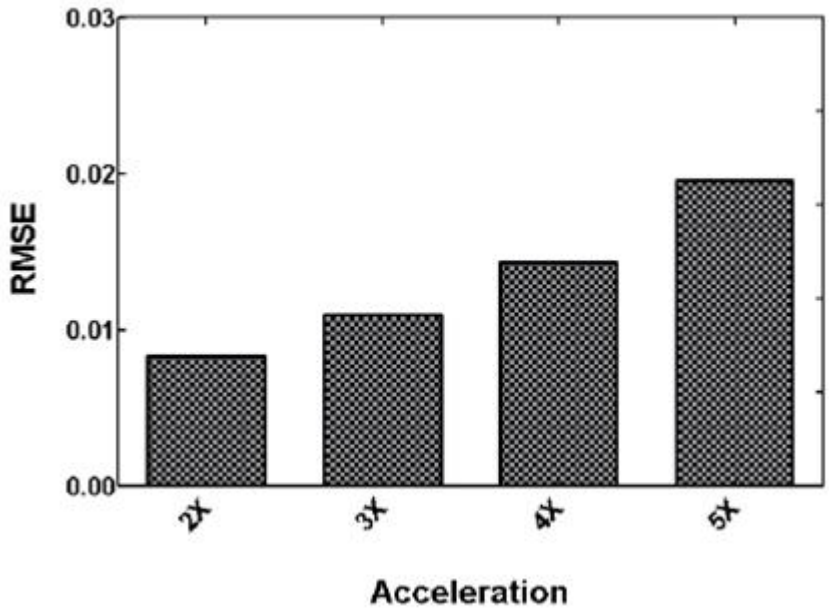

FIGURE 9. Voxel-weighted RMSE values for the reconstructions of the five knee data sets over acceleration factors of 2, 3, 4, and 5*x* as compared to 1*x*

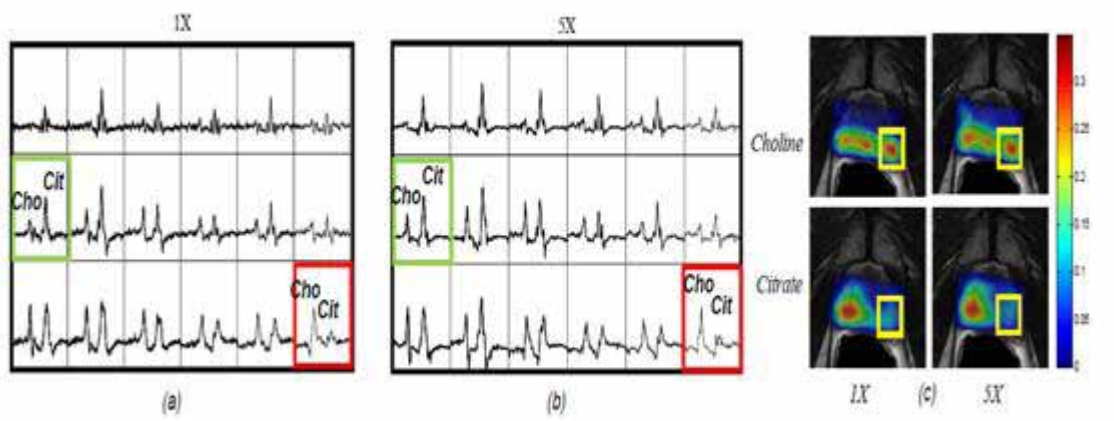

FIGURE 10. (a) Plot of the spectra of a representative prostate cancer MRSI at 1*x* (full *k*-space reconstruction); (b) an acceleration factor of 5 as compared to the original MRSI data (1*x*). Prostate cancer (shown in the red voxel) is characterized by increased choline (Cho) and reduced citrate (Cit) levels when compared to the metabolite profile of a normal prostate tissue (shown in green). (c) shows the Cho and Cit metabolite maps for the prostate cancer data at acceleration factors 1 and 5. The yellow boxes on the metabolite maps represent the location of the prostrate cancer.[41]

enhanced cardiovascular MR imaging, contrast-enhanced abdominal MR imaging, MR cholangiopancreatography, and knee MR imaging. Single 3D spoiled gradient-recalled acquisition in the steady state with Poisson disk sampling was obtained, with outer acceleration the degree at which undersampling is done outside of the central calibration region of the *k*-space. Gadolinium-based contrast agent was injected to acquire cardiovascular and abdominal acquisition. Highest acceleration was

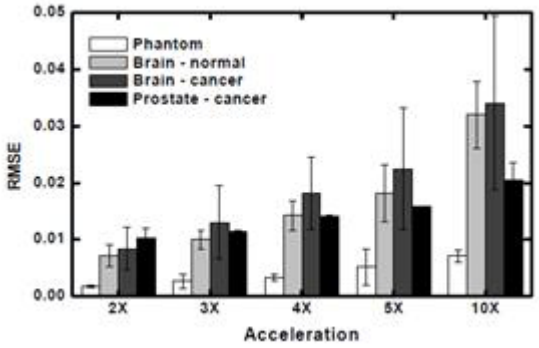

FIGURE 11. Graph of RMSE values for the different MRSI data used in the study as a function of acceleration factors of 2, 3, 4, 5, and 10

used to find size of the voxel, and knee examinations were performed without gadolinium-based contrast agent, and acceleration was used to decrease image time.

Two sets of images were reconstructed using standard PI and autocalibrating reconstruction for Cartesian sampling.[4] The 7 × 7 × 5 kernel was used for the above-mentioned and L_1 SPIR-iT method, with L_1 penalty parameter = 0.015. PI alone was generated on the imager and then transferred to the picture archiving and communication system, where as L_1 SPIR-iT was reconstructed in software programming language (Matlab; The Mathworks Inc, Massachusetts) and then transferred to the picture archiver. Two board-certified radiologists qualified in pediatric radiology (five and 20 years of clinical experience and MR imaging, respectively) viewed the two image series for each of 34 examinations in 34 patients (19 male and 15 female patients; mean age, 8.1 years; range, 0–17 years). The image quality of each image series was evaluated and rated by radiologist using a preference examination scale. Statistical analysis for the reconstructed image was done by using an exact Bowker test of symmetry. Statistical analyses were performed with statistical software on different method and different types..

Thirty-four examinations were done,[4] including L_1 chest MR angiographic, two abdominal MR angiographics, one extremity MR angiographic, one extremity MR venographic, six abdominal, five MR cholangiopancreatographic, and eight knee cartilage examinations on female patients (age range of 2–17 years) and male patients (age range 0–17 years). CS results were rated good and consistent in most of the examinations than in the autocalibrating reconstruction. A total of 325 structures were evaluated and approximately one-half of all structures were believed to have visual improvement and also not degraded by noise. Small structures, such as peripheral pulmonary arteries, and also soft tissue contrast was preserved in CS. A combination of CS and PI results in better reconstruction for all types of MR imaging including contrast-enhanced MRI using gadolinium as contrast agent, even in children, without suppressing the anatomic detail.

Low-power adiabatic pulses and a fast spiral acquisition technique were used to improve the MR spectroscopic imaging with more accurate localization and faster imaging.[42] The proposed technique was clinically evaluated on phantoms, five healthy volunteers, and five patients having glioblastoma using a 32-channel head coil on 3T MRI scanner. Localized adiabatic spin echo refocusing (LASER) by using adiabatic gradient-offset independent adiabaticity wideband uniform rate and smooth truncation (GOIA-W) was used for excitation with pulses with 3.5 ms duration, 20 kHz bandwidth, 0.81 kHz amplitude, and 45 ms echo time. After LASER excitation, conventional phase encoding (PE) was performed. Spectra acquired at similar spatial and temporal resolution using spiral encoding were compared with PE. Clinical evaluation proved that the spectroscopic images acquired at low spatial resolution was achieved four times faster, and at

higher spatial resolution, images were acquired two times faster using spiral protocol than the elliptical PE protocol. A SNR of 5 was obtained for the spiral protocol, which was adequate for distinguishing metabolites from noise.

CS and PI were combined by merging the *k-t* SPARSE technique with SENSE reconstruction to accelerate perfusion imaging.[43] Distributed CS theory framework has been proposed to understand the combination of *k-t* SPARSE with SENSE. The proposed framework identifies PI as a distributed multisensor implementation of CS, which estimate the feasible acceleration for the combined approach. First-pass cardiac perfusion MRI was performed on both male and female healthy volunteers (two males; ages 32 and 23) and one patient (male, age 38), with contrast agent. The proposed work demonstrates that eightfold acceleration can be achieved with whole heart coverage with high spatial and temporal resolution using standard coil array. The proposed method was highly insensitive to respiratory motion artifacts at eightfold acceleration compared to GRAPPA at twofold acceleration.

VI. OPEN SOURCE SOFTWARE FOR COMPRESSED SENSING

Open source tools for CS are typically built on Matlab. There are various tools such as Sparco,[44] Spgl,[45] Nesta,[46] and SMALLbox,[47] to name a few. Because sparsity is the major requirement of CS, a tool is required for testing the algorithms for sparse reconstruction, and Sparco can be used for this purpose.

Sparco is a framework for testing and benchmarking algorithms for sparse reconstruction. It includes a large collection of sparse reconstruction problems drawn from the imaging, CS, and geophysics literature. Sparco is also a framework for implementing new test problems and can be used as a tool for reproducible research. Sparco is implemented entirely in Matlab, and is released as open source software under the GNU public license.[44]

For the nonlinear reconstruction of images in CS, L_1 and L_2 problems must be solved. SPGL solves the basic pursuit problem required for nonlinear reconstruction in compress sensing and hence can be used as a tool for reconstruction. SPGL relies only on matrix-vector operations and accepts both explicit matrices and functions that evaluate these products. SPGL is suitable for problems that are in the complex domain. It can also be used to solve group sparsity problems.[45]

NESTA is a fast and robust first-order method that solves basis-pursuit problems and a large number of extensions (including TV denoising). The algorithm uses two ideas. The first idea is an accelerated convergence scheme for first-order methods, giving the optimal convergence rate for this class of problems. The second idea is a smoothing technique that replaces the nonsmooth L_1 norm with a smooth version. The algorithm basically solves the basis pursuit denoising problem.[46]

SMALLbox, a framework for sparse representation and dictionary learning. As an open source Matlab toolbox, SMALLbox can be seen as a tool for reproducible research in the sparse representations research community.[47]

VII. DISCUSSION

The successful application of CS to diverse methods of MRI as illustrated in this review reveals the significance of the technology. The increase in information content, specifically in terms of spatio-temporal resolutions and/or reduction in acquisition time, has had a significant impact in furthering MRI protocols in general and higher-dimensional MRI in particular. The applications of CS described in this review give an indication of the requirement by experts from different groups and the utility of this technique to solve varied challenges that MRI can address. However, evaluation of CS applications has to be furthered by clinical evaluations in cases of patient populations. The transition of CS as a technology to a tool in the clinic has also been pursued as has been pointed out in the section on clinical evaluation of CS in the case of pediatric population. Increased demonstration of the utility of CS in the clinic similar to the work described in the clinical evaluation section will aid rapid transition of CS as a clinically acceptable and understood standard to optimize MRI protocols. This will also provide confidence to radiologists about the tool and a platform to explore new avenues for accelerating MRI.

ACKNOWLEDGMENT

The authors acknowledge the support of Vision Group on Science and Technology - 5008/159718, 2013-14.

REFERENCES

1. Pruessmann, KP, Weiger M, Scheidegger MB, Boesiger P. SENSE: sensitivity encoding for fast MRI. Magn Resonance Med. 1999;42(5):952–62.
2. Candès EJ, Romberg J, Tao T. Robust uncertainty principles: Exact signal reconstruction from highly incomplete frequency information. IEEE Trans Inf Theory, 2006;52(2):489–509.
3. Lustig M, Donoho D, Pauly JM. Sparse MRI: the application of compressed sensing for rapid MR imaging. Magn Resonance Med. 2007;58(6):1182–95.
4. Vasanawala SS, Alley MT, Hargreaves BA, Barth RA, Pauly JM, Lustig M. Improved Pediatric MR Imaging with Compressed Sensing1. Radiology. 2010;256(2):607–16.
5. Candes EJ, Wakin MB, Boyd SP. Enhancing sparsity by reweighted ℓ 1 minimization. J Fourier Anal Appl. 2008;14(5-6):877–905.
6. Trzasko J, Manduca A. Highly Undersampled Magnetic resonance image reconstruction via homotopic< formula formulatype=. IEEE Trans Med Imaging. 2009;28(1):106–21.
7. Chartrand R. Fast algorithms for nonconvex compressive sensing: MRI reconstruction from very few data. In IEEE international symposium on biomedical imaging: from nano to macro, 2009. ISBI'09. Piscataway, NJ: IEEE; 2009. p. 262–5.
8. Lustig M, Donoho DL, Santos JM, Pauly JM. Compressed sensing MRI. IEEE Signal Process Mag. 2008;25(2):72–82.
9. Jung H, Ye JC, Kim EY. Improved k–t BLAST and k–t SENSE using FOCUSS. Phys Med Biol. 2007;52(11):3201–3235.
10. Gamper U, Boesiger P, Kozerke S. Compressed sensing in dynamic MRI. Magn Reson Med. 2008;59(2):365–73.
11. Jung H, Ye JC, Kim EY. Improved k–t BLAST and k–t SENSE using FOCUSS. Phys Med Boil. 2007;52(11):3201–3235.
12. Jung H, Sung K, Nayak KS, Kim EY, Ye JC. k–t FOCUSS: a general compressed sensing framework for high resolution dynamic MRI. Magn Reson Med. 2009;61(1):103–16.
13. Seeger M, Nickisch H, Pohmann R, Schölkopf B. Optimization of k–space trajectories for compressed sensing by Bayesian experimental design. Magn Reson Med. 2010; 63(1):116–26.
14. Bilgic B, Goyal VK, Adalsteinsson E. Multi–contrast reconstruction with Bayesian compressed sensing. Magn Reson Med. 2011;66(6):1601–15.
15. Liang D, DiBella EVR, ChenR–R, YingL. k–t ISD: Dynamic cardiac MR imaging using compressed sensing with iterative support detection. Magn Reson Med. 2012;68(1):41–53.
16. Usman M, Prieto C, Schaeffter T, Batchelor PG. k–t group sparse: a method for accelerating dynamic MRI. Magn Reson Med. 2011;66(4):1163–76.
17. Khare K, Hardy CJ, King KF, Turski PA, Marinelli L. Accelerated MR imaging using compressive sensing with no free parameters. Magn Reson Med. 2012;68(5):1450–7.
18. Vaswani N, Lu W. Modified-CS: Modifying compressive sensing for problems with partially known support. IEEE Trans Signal Process. 58, no. 9 (2010): 4595–607.
19. Sundaresan R, Kim Y, Nadar MS, Bilgin A. Motion-compensated compressed sensing for dynamic imaging. In: SPIE optical engineering+ applications. Bellingham, WA: SPIE; 2010. p. 77980A–77980A-8.
20. Liu B, Zou YM, Ying L. SparseSENSE: application of compressed sensing in parallel MRI. In: Information technology and applications in biomedicine. Piscataway, NJ: IEEE; 2008. p. 127–30.
21. Larkman DJ, Nunes RG. Parallel magnetic resonance imaging. Phys Med Biol. 2007;52(7):R15–R55.
22. Kim Y-C, Narayanan SS, Nayak KS. Accelerated 3D MRI of vocal tract shaping using compressed sensing and parallel imaging. Proceedings of ICASSP 2009. Piscataway, NJ: IEEE; 2009. p. 389–92.
23. Murphy M, Keutzer K, Vasanawala S, Lustig M. Clinically feasible reconstruction time for L1-SPIRiT parallel imaging and compressed sensing MRI. In: Proceedings of ISMRM Scientific Meeting & Exhibition.; 2010. p. 4854–4858.
24. Lustig M, Pauly JM. SPIRiT: iterative self–consistent parallel imaging reconstruction from arbitrary k–space. Magn Reson Med. 2010;64(2):457–71.
25. Wu B, Millane RP, Watts R, Bones PJ. Prior estimate–based compressed sensing in parallel MRI. Magn Reson Med. 2011;65(1):83–95.
26. Ilievska ES, Ivanovski ZA. Customized k-space trajectory for compressed sensing MRI. In: Telecommunications Forum (TELFOR), 19th. Piscataway, NJ: IEEE; 2011. p. 631–4.
27. Vandsburger MH, Epstein FH. Emerging MRI methods in translational cardiovascular research. J Cardiovasc Translat Res. 2011;4(4):477–92.
28. Kramer CM, Rogers WJ, Mankad S, Theobald TM, Pakstis DL, Hu Y-L. Contractile reserve and contrast uptake pattern by magnetic resonance imaging and functional recovery after reperfused myocardial infarction. J Am Col Cardiol. 2000;36(6):1835–40.
29. Bilen C, Selesnick IW, Wang Y, Otazo R, Kim D, Axel L, Sodickson DK. On compressed sensing in parallel MRI of cardiac perfusion using temporal wavelet and TV regularization. In: Acoustics speech and signal processing (ICASSP). Piscataway, NJ: IEEE; 2010. p. 630–3.
30. Otazo, Ricardo, Daniel Kim, Leon Axel, and Daniel K. Sodickson. "Combination of compressed sensing and parallel

imaging for highly accelerated first–pass cardiac perfusion MRI." *Magnetic Resonance in Medicine* 64, no. 3 (2010): 767-776.
31. Choyke PL, Dwyer, AJ, Knopp M. Functional tumor imaging with dynamic contrast-enhanced magnetic resonance imaging. J Magn Resonance Imaging. 2003;17(5):509–20.
32. Ji J, Lang T. Dynamic MRI with compressed sensing imaging using temporal correlations. Piscataway, NJ: IEEE; 2008. pp. 1613–6.
33. Geethanath S, Gulaka PK, Kodibagkar VD, A comparative study of undersampling schemes for magnetic resonance dynamic contrast enhanced imaging, Proceedings of ISMRM Annual Meeting, Montreal. Mag Reson Med; 2011. p. 2630-2630.
34. Milles J, Versluis MJ, Webb AG, Reiber JHC. Quantitative evaluation of compressed sensing in MRI: application to 7T time-of-flight angiography. In: Information technology and applications in biomedicine. Piscataway, NJ: IEEE; 2010. p. 1–4.
35. de Zwart JA, van Gelderen P, Kellman P, Duyn JH. Application of sensitivity-encoded echo-planar imaging for blood oxygen level-dependent functional brain imaging. Magn Reson Med. 2002;48(6): pp. 1011–20.
36. Jung H, Jong Chul Ye. Performance evaluation of accelerated functional MRI acquisition using compressed sensing. In: Biomedical imaging: from nano to macro. Piscataway, NJ: IEEE; 2009. p. 702–5.
37. Doneva M, Börnert P, Eggers H, Stehning C, Sénégas J, Mertins A. Compressed sensing reconstruction for magnetic resonance parameter mapping. Magn Reson Med. 2010;64(4):1114–20.
38. Jensen LR, Garzon B, Heldahl MG, Bathen TF, Lundgren S, Gribbestad IS. Diffusion-weighted and dynamic contrast-enhanced MRI in evaluation of early treatment effects during neoadjuvant chemotherapy in breast cancer patients. J Magn Reson Imaging. 2011;34(5):1099–109.
39. Yihang Zhou, Yanhua Wang, Leslie, A Kernel-based compressed sensing approach to dynamic MRI from highly undersampled data. Proceedings of 35th IEEE Annual Conference on Engineering in Medicine and Biology; Kyoto. Piscataway, NJ: IEEE. http://www.acsu.buffalo.edu/~jlv27/index_files/Publications_files/A%20KERNEL-BASED%20CS%20APPROACH%20TO%20DYNAMIC%20MRI.pdf; p. 1–4.
40. Geethanath S, Moeller S, Kodibagkar VD, Accelerated 3D radial short echo-time MRI of the knee using compressed sensing. Proceedings of ISMRM Annual Meeting; Melbourne, Australia. Mag Reson Med; 2012. p. 3286-3286.
41. Geethanath S, Baek H-M, Ganji SK, Ding Y, Maher EA, Sims RD, Choi C, Lewis MA, Kodibagkar VD. Compressive sensing could accelerate 1H MR metabolic imaging in the Clinic 1, Radiology. 2012;262(March):985-994.
42. Andronesi OC, Gagoski BA, Sorensen AG. Neurologic 3D MR spectroscopic imaging with low-power adiabatic pulses and fast spiral acquisition. Radiology. 2012;262(2):647–61.
43. Otazo R, Kim D, Axel L, Sodickson. Combination of compressed sensing and parallel imaging for highly accelerated first-pass cardiac perfusion MRI. Magn Reson Med. 2010;64(3):767–76.
44. Ewout van den Berg, Michael P. Friedlander, Gilles Hennenfent, Felix J. Herrmann, Rayan Saab and Özgür Yilmaz. Algorithm 890: {Sparco}: A Testing Framework for Sparse Reconstruction. [cited 2013 06 18]. Available from: www.cs.ubc.ca/~mpf/2009-sparco.html
45. Michael P. Friedlander and Ewout van den Berg. [cited 2013 06 18]. Available from: http://www.cs.ubc.ca/~mpf/spgl1/
46. Jérôme Bobin and Stephen Becker. [cited 2013 06 18]. Available from: www-stat.stanford.edu/~candes/nesta/
47. Rémi Gribonval. [cited 2013 06 18]. Available from: http://small-project.eu/software-data/smallbox/.